Iraqi Journal of Scientific and Industrial Research
Volume 3, Issue (3), July-September 2024, pp. 5-8

Stable and Overloaded Functional Characteristics of Anticorrosive Alloys Employed for Turbo Engine Assembly

Jonas M. Bordon

Department of Mechanical Engineering, Faculty of Engineering, University of Rotterdam, Rotterdam, THE NETHERLANDS

Abstract

In this work, the functional characteristics of the anticorrosive alloys employed for turbo engine assembly were introduced. They were analyzed under two separate conditions; stable and overloaded. This analysis is based on the evaluation of net product of the engine consumption cycle as well as the retraction factor over time. The stable functional characteristics showed that the anticorrosive alloy may be exerted to a periodic load that may suddenly cause a degradation when correlated to the thermal effect resulted from operation. On the other hand, the overloaded functional characteristics showed that the anticorrosive alloy may avoid any degradation when the operation is periodically interrupted.

Keywords: Dynamic analysis; MIS devices; Power electronics; Charge separation

Received: 4 April 2024; **Revised:** 9 July 2024; **Accepted:** 16 July 2024; **Published:** 1 October 2024

1. Introduction

The dynamically developing industrial sectors, such as the aerospace industry, the space industry, or the energy industry aim at increasing the efficiency and longer lifespan of components working in difficult operating conditions, such as high temperatures, aggressive environments, and reactions with gases, liquids, and solids. Therefore, materials that can operate in extreme conditions are still developed.

Modern technology has made intensive use and employment of the turbo engines, which provide higher momenta within shorter periods and relatively lower costs. However, the assemblies of the turbo engines still require complex technology and sophisticated integration with the conventional or fundamental configurations of mechanical and dynamic systems. Research works have been continued to replace the corrosive parts of the engines with others made from anticorrosive alloys, mainly Zn-Ni alloys.

The Zn-Ni anticorrosive coating performance mainly depends on the concentration of the metals in the alloy. The electrodeposition of these alloys has three phases: alpha, beta, and gamma. The alpha is a solid solution of zinc in nickel, while the gamma phase is a solid solution of nickel in zinc. The beta phase is an intermediate between the aforementioned phases. Figure (1) shows the phase diagram of a binary Zn-Ni system.

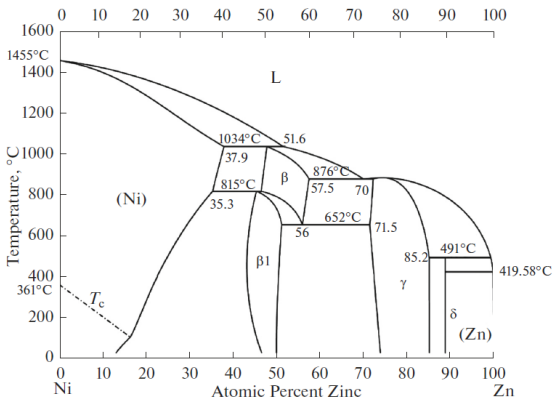

Fig. (1) Calculated phase diagram of a binary Ni-Zn system

The Zn-Ni alloys applied as anticorrosive steel coatings generally have Zn composition of 85-99%. Thus, the substance has anodic potential compared to the substrate, however, it is less active compared to pure Zn.

The Zn-Ni alloys do not require a layer of chromate, which is toxic to the environment. Any percentage increase in the composition of nickel in the alloy occurs due to a high proportion of the concentration of Ni compared to Zn. The pure Zn-Ni alloys were deposited on AISI 347 steel electrodes using direct current and pulsed current at a temperature of 50 °C, pH level of 2.5, and different electrolytes. The alloy with the best anticorrosive result, with corrosion current of 10 μA/cm^2 was obtained by pulsed current and presented a uniform and granular surface, composed of small grains and low porosity.

2. Experimental Work

AISI 347 steel gearboxes were coated with Zn-Ni alloy with different thickness using pulsed current coating system. The coefficient of performance of the coated gearboxes was compared to that of uncoated gearbox (see Fig. 2). The operation was evaluated at room temperature as well as elevated temperatures in order to simulate the practical environment.

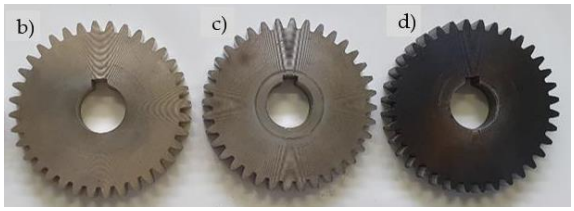

Fig. (2) Uncoated and coated gearbox parts used for the comparison of this work

The stable and overloaded functional characteristics of the anticorrosive alloys employed for coating of the gearbox parts were introduced (see Fig. 3) and compared as the surrounding temperature was ranging from room temperature to 100°C.

Fig. (3) Measurement setup of the gearbox parts

The operation periods were ranging from 10 min to 2 hours as continuous operation and 6 hours as interrupted operation. All mechanical and thermodynamics parameters were determined.

3. Results and Discussion

The analysis coefficient of operation (COP) under the stable condition can be determined as follows [26]:

$$COP = \frac{NT_{pg}}{1440 - T_{pr}} \quad (1)$$

where N is the throughput capacity of the line section, T_{pg} is the graph period, and T_{pr} is the time of technological downtime

The COP under the overloaded condition is determined by the following formula:

$$COP = \frac{\sum_{i=1}^{n} N_i T_i}{1440 - T_{pr}} \quad (2)$$

where T_i is the time periods over which the operation is conducted, and N_i is the number of measurement steps over the operation period

Figure (4) shows the time-dependent behavior of the coefficient of operation (COP) of uncoated gearbox under the conditions of stable and overloaded functional characteristics. The latter condition is actually containing two components; positive or incremental overload operation and negative or decremented overload operation. The functional characteristics reasonably depend on the role of Zn-Ni coating to dissipate the generated heat, minimize the friction, and finally exclude the static charge accumulation. It is desired to operate the gearbox under the positive overloaded condition (blue curve) but the correlation to the negative overloaded condition is unavoidable. Therefore, the stable condition may be considered as the optimum choice despite the disadvantages mentioned before. Consequently, the characterization of the coated gearboxes would assist better choice.

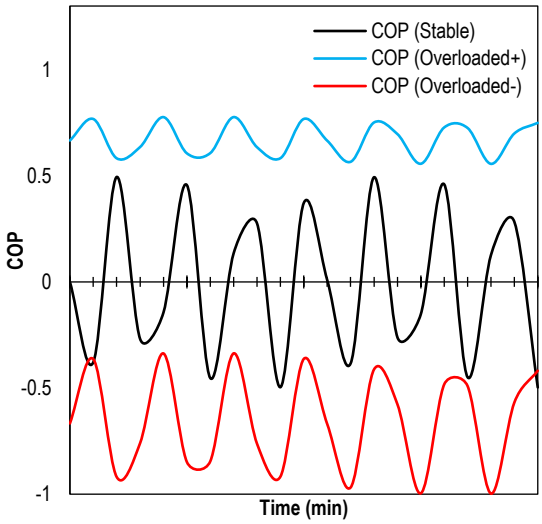

Fig. (4) Time-dependent behavior of COP of uncoated parts under the three different conditions considered in this work

Figure (5) shows the time-dependent behavior of the coefficient of operation (COP) of gearbox coated with Zn-Ni alloy under the conditions of stable and overloaded functional characteristics. The behavior

of COP under the positive overloaded condition was not largely different from the previous case (uncoated parts), while the negative overloaded condition exhibits reasonable difference. On the other hand, the stable condition shows higher amplitudes of the COP function. This may be optimum choice for the practical purposes but, actually, it imposes higher stress on the gearbox and hence makes it difficult to achieve the advantages of the Zn-Ni coating.

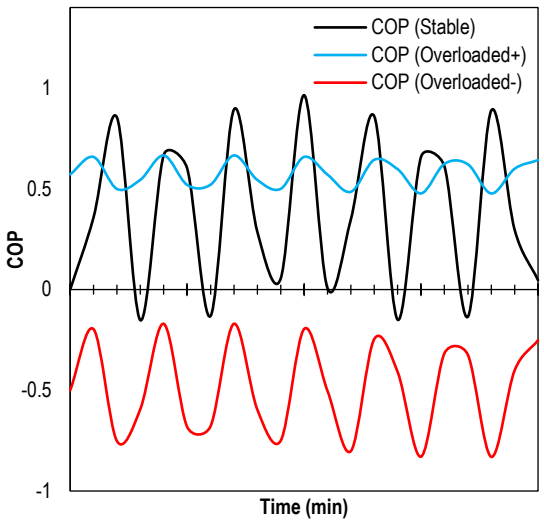

Fig. (5) Time-dependent behavior of COP of coated parts under the three different conditions considered in this work

The difference between the coated and uncoated parts can be clearly shown by the area-under-curve, as shown in Fig. (6). Choosing the coating with Zn-Ni alloy is restricted by both mechanical and thermodynamic roles of this coating. Therefore, an analysis of these properties is required as individual and correlated parameters.

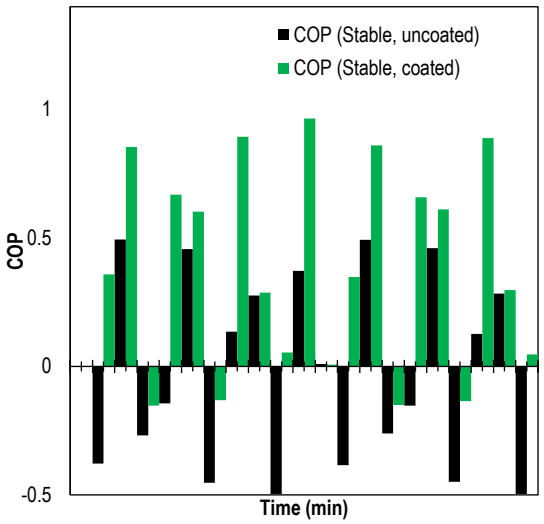

Fig. (5) Comparison of time-dependent stable behavior of COP of coated and uncoated parts

4. Conclusion

Based on the results obtained from this work, it can be concluded that the employment of Zn-Ni alloy coatings on the parts in turbo engine assemblies provides better ability to hold the mechanical and thermal stresses resulted from the operation. Stable functional characteristics of the coated parts was found reasonably better than the overloaded functional characteristics for practical uses.

References

[1] M. Brzhezinskaya et al., "Large-scalable graphene oxide films with resistive switching for non-volatile memory applications", *J. Alloys Comp.*, 849 (2020) 156699.

[2] A.P. Patil et al., "Tuning the analog and digital resistive switching properties of TiO_2 by nanocompositing Al-doped ZnO", *Mater. Sci. Semicond. Process.*, 115 (2020) 105110.

[3] T.M. Rawson et al., "Artificial intelligence can improve decision-making in infection management", *Nat. Hum. Behav.*, 3(6) (2019) 543-545.

[4] Z. Shen et al., "Advances of RRAM Devices: Resistive Switching Mechanisms, Materials and Bionic Synaptic Application", *Nanomater. (Basel)*, 10(8) (2020) 1437.

[5] C. Fernandez et al., "Comprehensive predictive modeling of resistive switching devices using a bias-dependent window function approach", *Solid-State Electron.*, 170 (2020) 107833.

[6] Y. Liu et al., "Effect of film thickness and temperature on the resistive switching characteristics of the Pt/HfO_2/Al_2O_3/TiN structure", *Solid-State Electron.*, 173 (2020) 107880.

[7] H.T. Kwon et al., "Resistive random-access memory with an a-Si/SiN_x double-layer", *Solid-State Electron.*, 158 (2019) 64-69.

[8] Y.F. Qi et al., "Resistive switching behavior of solution-processed AlO_x and GO based RRAM at low temperature", *Solid-State Electron.*, 168 (2020) 107735.

[9] R.W.a.I. Valov, "Electrochemical Reactions in Nanoionics-Towards Future Resistive Switching Memories", *ECS Trans.*, 25(6) (2009) 431-437.

[10] X.D. Huang et al., ""'Enhancement of DC/AC resistive switching performance in AlO_x memristor by two-technique bilayer approach", *Appl. Phys. Lett.*, 116(17) (2020) 73504.

[11] Z. Shen et al., "Effect of Annealing Temperature for Ni/AlO_x/Pt RRAM Devices Fabricated with Solution-Based Dielectric", *Micromach. (Basel)*, 10() (2019) 446.

[12] H.W. Shin and J.Y. Son, "Resistive switching characteristics of graphene/NiO/highly ordered pyrolytic graphite resistive random access

memory capacitors", *J. Alloys Comp.*, 772 (2019) 900-904.
[13] X. Kang et al., "NiO-based resistive memory devices with highly improved uniformity boosted by ionic liquid pre-treatment", *Appl. Surf. Sci.*, 480 (2019) 57-62.
[14] H. Ryu, J. Choi and S. Kim, "Voltage Amplitude-Controlled Synaptic Plasticity from Complementary Resistive Switching in Alloying HfO_x with AlO_x-Based RRAM", *Metals*, 10(11) (2020) 1410.
[15] J. Sun, J.B. Tan and T. Chen, "HfO_x-Based RRAM Device With Sandwich-Like Electrode for Thermal Budget Requirement", *IEEE Trans. Electron Dev.*, 67(10) (2020) 4193-4200.
[16] J. Kim et al., "Recent Progress of Quantum Dot□based Photonic Devices and Systems: A Comprehensive Review of Materials, Devices, and Applications", *Small Struct.*, 59 (2020) 1-57.
[17] X. Hong et al., "Oxide-based RRAM materials for neuromorphic computing", *J. Mater. Sci.*, 53(12) (2018) 8720-8746.
[18] X. Cao et al., "Enhanced Switching Ratio and Long-Term Stability of Flexible RRAM by Anchoring Polyvinylammonium on Perovskite Grains", *ACS Appl. Mater. Interfac.*, 11(39) (2019) 35914-35923.
[19] H. Wang and X. Yan, "Overview of Resistive Random Access Memory (RRAM): Materials, Filament Mechanisms, Performance Optimization, and Prospects", *phys. stat. sol. (RRL) Rapid Res. Lett.*, 13(9) (2019) 1900073.
[20] V. Gupta et al., "Resistive Random Access Memory: A Review of Device Challenges", *IETE Tech. Rev.*, 37(4) (2019) 377-390.
[21] K. Moon et al., "RRAM-based synapse devices for neuromorphic systems", *Faraday Discuss*, 213 (2019) 421-451.
[22] K. Bejtka et al., "TEM Nanostructural Investigation of Ag-Conductive Filaments in Polycrystalline ZnO-Based Resistive Switching Devices", *ACS Appl. Mater. Interfac.*, 12(26) (2020) 29451-29460.
[23] C.-C. Hsu, P.-X. Long and Y.-S. Lin, "Enhancement of Resistive Switching Characteristics of Sol-Gel TiO_x RRAM Using Ag Conductive Bridges", *IEEE Trans. Electron Dev.*, (2020) 1-8.
[24] Q. Liu et al., "Formation of multiple conductive filaments in the Cu/ZrO_2:Cu/Pt device", *Appl. Phys. Lett.*, 95(2) (2009) 023501-1-023501-4.
[25] B. Sun et al., "Effect of Cu ions assisted conductive filament on resistive switching memory behaviors in $ZnFe_2O_4$-based devices", *J. Alloys Comp.*, 694 (2017) 464-470.
[26] M. Huang et al., "Global-gate controlled one-transistor one-digital-memristor structure for low-bit neural network", *IEEE Electron Dev. Lett.*, 10 (2020) 1-4.
[27] X.-D. Huang et al., "Forming-Free, Fast, Uniform, and High Endurance Resistive Switching From Cryogenic to High Temperatures in W/AlO_x/Al_2O_3/Pt Bilayer Memristor", *IEEE Electron Dev. Lett.*, 41(4) (2020) 549-552.
[28] J. Liu et al., "Science and Technology of Integrated Super-High Dielectric Constant AlO_x/TiO_y Nanolaminates / Diamond for MOS Capacitors and MOSFETs", *Carbon*, 172 (2021) 112-121.
[29] S. Yu, X. Guan and H.S.P. Wong, "On the Switching Parameter Variation of Metal Oxide RRAM—Part II: Model Corroboration and Device Design Strategy", *IEEE Trans. Electron Dev.*, 59(4) (2012) 1183-1188.
[30] S. Liu et al., "Significant Effects of Electrode Metal Work Function on Resistive Memory Devices with Gelatin Biodielectric Layer", *J. Electrochem. Soc.*, 165(7) (2018) G90-G95.
[31] S.M. Hong et al., "Effect of Work Function Difference Between Top and Bottom Electrodes on the Resistive Switching Properties of SiN Films", *IEEE Electron Dev. Lett.*, 34(9) (2013) 1181-1183.

